Supplementary data:

Table of Contents:

All metabolite changes detected in the study: Each metabolite was identified using a PLS-DA model with jack knifing used to assess the contribution of that metabolite to the first component using a 95% limit. In addition data sets were analysed by a univariate analysis (Student t-test) with (**) and without (*) a Bonferoni correction at the 95% limit. Typically 100-130 peaks were detected in the aqueous GC-MS data, 221 integral regions and the GC-MS lipid data 85 peaks, of which 29 were identified as fatty acid methyl esters.

Age	**Aqueous GC-MS Data**		**NMR Data**	
	Increase in PPAR-α$^{-/-}$	*Decrease in PPAR-α$^{-/-}$*	*Increase in PPAR-α$^{-/-}$*	*Decrease in PPAR-α$^{-/-}$*
3m	*N/A*	Disaccharide * Glucose ** Malate Phenylalanine Fumarate Glycine * Threonine * Myo-Inositol *	Glycerol * Taurine *	Alanine * Leucine/ Isoleucine * Glucose **
5m	Sugar 5-oxo-proline * Malate Alanine Citrate * Glycine Fumarate Glutamate **	Lactate * Disaccharide Glucose *	-$CH_2CH_2CH_2$- *	Glucose *
7m	Sugar Disaccharide Threonate Fumarate	Disaccharide Succinate * Phosphorylated sugar Glycerophosphoric acid Citrate Alanine Glucose *	Taurine * Betaine *	Glucose * Alanine
9m	4-aminobutyric acid Alanine * Sugar Valine * Proline * Threonine	Sugar Glucose *	Taurine * PC/ GPC * Isoleucine Glutamine *	Glucose * Glycogen * ANPs ** Glycine *
11m	Sugar Threonate 5-oxo-proline *	Sugar Proline Cholesterol * Glucose *	Isoleucine * Creatine * Glycine *	PC/ GPC * Betaine * Glucose *
13m	Sugar Urea Phosphorylated sugar Threonate	Phenylalanine Glucose ** Ornithine Glutamine * Alanine Glutamate * Citrate	Taurine * Lactate *	Glucose ** Glycogen ** ANPs *

Table 1: Summary of the metabolic perturbations identified between samples of wild type and PPAR-α null liver tissue. Metabolite changes were detected by multivariate analysis following the analysis of aqueous tissue extracts by both GC-MS and ^{1}H NMR spectroscopy. The concentration of metabolites listed here was found to differ significantly between wild type and PPAR-α null samples at the 95 % confidence limit.

Age	Aqueous GC-MS Data		NMR Data	
	Increase in PPAR-α$^{-/-}$	*Decrease in PPAR-α$^{-/-}$*	*Increase in PPAR-α$^{-/-}$*	*Decrease in PPAR-α$^{-/-}$*
3m	Fumarate Malate Sugar (ID unknown)	Uridine 9H-purine Creatine Glycerol Glycine	Lactate Alanine	Taurine Creatine
5m	Malate Glutamate Fumarate 5-oxo-proline Threonate Sugar Myo-Inositol Phosphorylated Sugar Aspartate 9H-purine *	Linoleic Acid Lactate * Disaccharide β-hydroxybutyrate	Glutamate/ Glutamine PC/ GPC	Lactate * Creatine Alanine ATP *
7m	Fumarate Lactate *	Valine Phenylalanine Alanine Citrate Threonine Creatine * Proline * Glutamate * Glycine	Lactate *	Creatine * PC/ GPC * ATP *
9m	Glutamine * Myo-Inositol * Fumarate	Succinate β-hydroxybutyrate * Sugar	*N/A*	*N/A*
11m	Fumarate Threonate Glyceric Acid Phosphorylated Sugar Malate	Lactate Succinate	*N/A*	ATP * Lactate
13m	Fumarate Myo-Inositol Glutamate 4-aminobutyric acid Phenylalanine	Succinate Glyceric Acid Uridine	Taurine Glutamate/ Glutamine	Lactate * Creatine * GPC/ PC * *Unassigned* @ 3.12 * ATP

Table 2: Summary of the metabolic perturbations identified between samples of wild type and PPAR-α null heart tissue. Metabolite changes were detected by multivariate analysis following the analysis of aqueous tissue extracts by both GC-MS and ^{1}H NMR spectroscopy. The concentration of metabolites listed here was found to differ significantly between wild type and PPAR-α null samples at the 95 % confidence limit.

Age	Aqueous GC-MS Data		NMR Data	
	Relative increase	*Relative decrease*	*Relative increase*	*Relative decrease*
3m	*N/A*	*N/A*	CH3CH2- Alanine *	Lactate
5m	Gluconic Acid Sugar Ornithine Serine Glycine	Sugar Unsaturated Fat * Acetic Acid Alanine Lactate	-CH2CH2CH2- *	
7m	Acetic Acid Lactate * Beta-alanine Valine	1-monopalmitin * Unsaturated Fat * Glucose Sugar 17:0 FA *	Taurine PC/ GPC -CH3 * Choline	-CH2CH2CH2- * -COCH2- *
9m	Sugar Cholesterol Serine Sugar 17:0 FA 18:0 FA Fumarate Sugar	Beta hydroxybutyrate * Isoleucine * Acetic Acid 12:0 FA 16:1 FA	*N/A*	*N/A*
11m	Sugar 16:1 FA Gluconic Acid Cholesterol 14:0 FA	Disaccharide Sugar Unsaturated Fat Creatine * Inositol Isomer Glucose *	Lactate	PC/ GPC * Glucose *
13m	18:0 FA 1-monostearate Cholesterol 16:0 FA 9:0 FA 18:1 FA 18:2 FA	Unsaturated Fat Sugar Creatine * Glucose	-CH2CH2CH2- -COCH2- PC/GPC	Glucose

Table 3: Summary of the metabolic perturbations identified between samples of wild type and PPAR-α null white adipose tissue. Metabolite changes were detected by multivariate analysis following the analysis of aqueous tissue extracts by both GC-MS and ^{1}H NMR spectroscopy. The concentration of metabolites listed here was found to differ significantly between wild type and PPAR-α null samples at the 95 % confidence limit.

Age	Aqueous GC-MS Data		NMR Data	
	Increase in PPAR-α$^{-/-}$	*Decrease in PPAR-α$^{-/-}$*	*Increase in PPAR-α$^{-/-}$*	*Decrease in PPAR-α$^{-/-}$*
3m	Glycine * Malate * Fumarate Uridine * Lactate * Disaccharide Citrate *	Glycerophosphoric acid Threonate Glutamate **	Alanine ** Glycine **	Creatine ** Taurine **
5m	Myo-Inositol Malate Fumarate Citrate Phosphorylated sugar	Phenylalanine * Phosphoric acid	Lactate * Alanine	Creatine
7m	Uridine Ornithine Myo-Inositol Phosphoric Acid	Glucose * Phosphorylated Sugar Glutamate *	Taurine Alanine Glycine	Choline Lactate Creatine
9m	Ornithine Valine Phosphorylated Sugar Succinate	Malate Urea Glucose * Citrate Phenylalanine Glutamate Creatine * Fumarate	Alanine Adenosine *	Choline * Phosphocreatine * *Not assigned* (δ3.74) * PC/ GPC * Aspartate Lactate * ATP *
11m	Phosphoric acid Stearic acid	Urea Sugar Creatine Myo-Inositol Fumarate Proline Lactate Citrate	Glycine * Phosphocreatine Acetate Leucine/ Lysine *	Creatine Lactate ATP * Malate
13m	Alanine Sugar Phosphorylated sugar Serine Valine Proline Urea Aspartate	Citrate Ornithine Tyrosine Gluconic acid Fumarate Creatine Malate	Alanine	Creatine *Not assigned* (δ3.74) Lactate ATP *

Table 4: Summary of the metabolic perturbations identified between samples of wild type and PPAR-α null gastrocnemius skeletal muscle tissue. Metabolite changes were detected by multivariate analysis following the analysis of aqueous tissue extracts by both GC-MS and ^{1}H NMR spectroscopy. The concentration of metabolites listed here was found to differ significantly between wild type and PPAR-α null samples at the 95 % confidence limit.

Age	**Aqueous GC-MS Data**		**NMR Data**	
	Increase in PPAR-α$^{-/-}$	*Decrease in PPAR-α$^{-/-}$*	*Increase in PPAR-α$^{-/-}$*	*Decrease in PPAR-α$^{-/-}$*
3m	Sugar * Palmitic Acid Fumarate Myo-Inositol *	*N/A*	*N/A*	Creatine Taurine Lactate Choline Acetate
5m	Disaccharide *	*N/A*	Lactate *	Creatine * Acetate *
7m	*N/A*	*N/A*	Lactate Succinate PC/ GPC	Creatine
9m	*N/A*	Creatine	PC/ GPC	Lactate Adenosines * Glycine
11m	Disaccharide	Stearic Acid Creatine * Threonine Valine 5-oxo-proline Palmitic Acid Serine	Lactate Alanine	Creatine *
13m	Sugar	Glucose * Galactose	Taurine * Lactate	Glycine * Creatine

Table 5: Summary of the metabolic perturbations identified between samples of wild type and PPAR-α null soleus skeletal muscle tissue. Metabolite changes were detected by multivariate analysis following the analysis of aqueous tissue extracts by both GC-MS and ^{1}H NMR spectroscopy. The concentration of metabolites listed here was found to differ significantly between wild type and PPAR-α null samples at the 95 % confidence limit.

Age	Aqueous GC-MS Data		NMR Data	
	Increase in PPAR-α$^{-/-}$	*Decrease in PPAR-α$^{-/-}$*	*Increase in PPAR-α$^{-/-}$*	*Decrease in PPAR-α$^{-/-}$*
3m	Sugar * Gluconic Acid Fumarate Citrate	Myo-Inositol *	Lactate * Glutamate/Glutamine *	Leucine * Taurine Creatine
5m	Citrate * Hydroxyproline Lactate * Disaccharide	Gluconic Acid	Lactate *	Glycerol *
7m	Hydroxyproline	*N/A*	*N/A*	*N/A*
9m	*N/A*	Glyceric Acid Glucose Fumarate	Lactate * Creatine Taurine	Glycine Valine Glutamate/ Glutamine Glucose
11m	Sugar Succinate	Glucose	Creatine	Phosphocreatine Glycine
13m	Hydroxyproline Disaccharide Myo-Inositol Threonate Sugar	Sugar Glucose * Phosphorylated Sugar	*N/A*	Glucose * Taurine *

Table 6: Summary of the metabolic perturbations identified between samples of wild type and PPAR-α null diaphragm tissue. Metabolite changes were detected by multivariate analysis following the analysis of aqueous tissue extracts by both GC-MS and ^{1}H NMR spectroscopy. The concentration of metabolites listed here was found to differ significantly between wild type and PPAR-α null samples at the 95 % confidence limit.

Age	*Increase in PPAR-α $^{-/-}$*	*Decrease in PPAR-α $^{-/-}$*
3m	15:0 10c- 15:1 20:0 ** 9c- 14:1 16:1 * 15:0 (Branched chain) 18:1 *	*N/A*
5m	9c, 12c-18:2 20:0	9c-18:1 * 16:0 (Branched chain) 16:0 (Branched chain)
7m	18:0 20:0 * 9c, 12c-18:2	8c, 11c, 14c-20:3
9m	18:0 16:0 19:0	9c-18:1 * 16:1
11m	20:0 18:0 9c, 12c-18:2 8c, 11c, 14c-20:3	16:0 ** 12:0
13m	9c-18:1 * 9c, 12c-18:2 8c, 11c, 14c-20:3	17:0 (Branched) 16:0 **

Table 7: Summary of hepatic organic metabolic perturbations detected by multivariate analysis between wild type and PPAR-α null mice aged between 3 and 13 months. The metabolites listed significantly contribute to class separation at the 95 % confidence limit. Unless stated double bond locations are unknown.

Age	*Relative increase*	*Relative decrease*
3m	9c, 12c-18:2	6c, 9c, 12c-18:3 9c-16:1 * 10c-17:1 14:0 15:0 16:1 18:0 (Branched Chain)
5m	9c, 12c-18:2 11c, 14c-20:2 9c-14:1	14:0 18:0 (Branched Chain) 10c-15:1 16:0 9c-16:1 * 6c, 9c, 12c-18:3
7m	9c, 12c-18:2 9c-18:1 * 20:0	24:0 6c, 9c, 12c-18:3 11c-20:1 8c, 11c, 14c-20:3 13c-22:1 9c-16:1 * 15:0 (Branched Chain) 4c, 7c, 10c, 13c, 16c, 19c-22:6
9m	9c-18:1 * 9c, 12c-18:2	24:0 * 18:0 (Branched Chain) 19:0 (Branched Chain) 10c-15:1 4c, 7c, 10c, 13c, 16c, 19c-22:6 22:0
11m	9c-18:1 * 9c, 12c-18:2	24:0 18:0 (Branched Chain) 11c-20:1 6c, 9c, 12c-18:3
13m	16:0 9c, 12c-18:2 19:1	24:0 5c, 8c, 11c, 14c-20:4 8c, 11c, 14c-20:3 18:0 (Branched Chain) 6c, 9c, 12c-18:3 14:0

Table 8: Summary of cardiac organic metabolic perturbations detected by multivariate analysis between wild type and PPAR-α null mice aged between 3 and 13 months. The metabolites listed significantly contribute to class separation at the 95 % confidence limit. Unless stated double bond locations are unknown.

Age	FAME GC-MS Data	
	Relative increase	*Relative decrease*
3m	18:0	10c-15:1
	11c, 14c-20:2	9c- 14:1
		16:0 (Branched chain)
		9c-16:1
5m	11c, 14c-20:2	17:0 (Branched Chain)
	16:1	9c-16:1
	18:0	18:0 (Branched Chain)
	15:0	10:0
	6:0	9c-14:1
	20:0	
	19:0 (Branched)	
	13c, 16c-22:2	
7m	11c, 14c-20:2	17:0
	20:0	9c-16:1
	18:0	10c-17:1
	10c-15:1	16:1
	17:0	18:0 (Branched Chain)
	24:0	4c, 7c, 10c, 13c, 16c, 19c-22:6
	8c, 11c, 14c-20:3	
	15:1	
9m	11c, 14c-20:2	18:0 (Branched Chain)
	14:0	17:0 (Branched Chain)
	12:0	10c-17:1
	10:0	9c-16:1
	13:0	4c, 7c, 10c, 13c, 16c, 19c-22:6
	18:0	
11m	12:0	9c, 12c-18:2
	10:0	9c-16:1
	10:1	16:1
	11c, 14c-20:2	18:0 (Branched Chain)
	8c, 11c, 14c-20:3	17:0 (Branched Chain)
		15:0
		4c, 7c, 10c, 13c, 16c, 19c-22:6
13m	11c, 14c-20:2	18:0
	8c, 11c, 14c-20:3	4c, 7c, 10c, 13c, 16c, 19c-22:6
	16:2	8:0
	6c, 9c, 12c-18:3	14:0
	17:0	12:0
	16:0	10:0

Table 9: Summary of WAT organic metabolic perturbations detected by multivariate analysis between wild type and PPAR-α null mice aged between 3 and 13 months. The metabolites listed significantly contribute to class separation at the 95 % confidence limit. Unless stated double bond locations are unknown.

Age trend of fatty acid profiles in adipose tissue

To examine how age interacts with PPAR-α null status in terms of total fatty acid metabolism in adipose tissue the multivariate regression technique PLS was applied to the whole, control and PPAR-α null fatty acid methyl ester datasets. For all three datasets robust models were built (Q^2 = 0.34, 0.50 and 0.34, respectively) (**Fig Sup 1a & 1b**). Of the identified fatty acids, ageing was associated with decreases in the relative concentration of 15:1 pentadecenoic acid, 22:2 (n-6) docasadienoic acid and 16:1 (n-10) hexadecenoic (sapienic) acid and increases in 11:0 undecanoic acid, 22:0 docasanoic acid, 16:1 (n-7) hexadecenoic (palmitoleic acid), and 16:2 hexadecenoic acid across the combined dataset.
Across all three models the similarity of these ageing trends were further characterised by the fact that the PLS model formed from the control data was also predictive for the PPAR-α null mice (**Sup Fig 1c**).

Fig1a

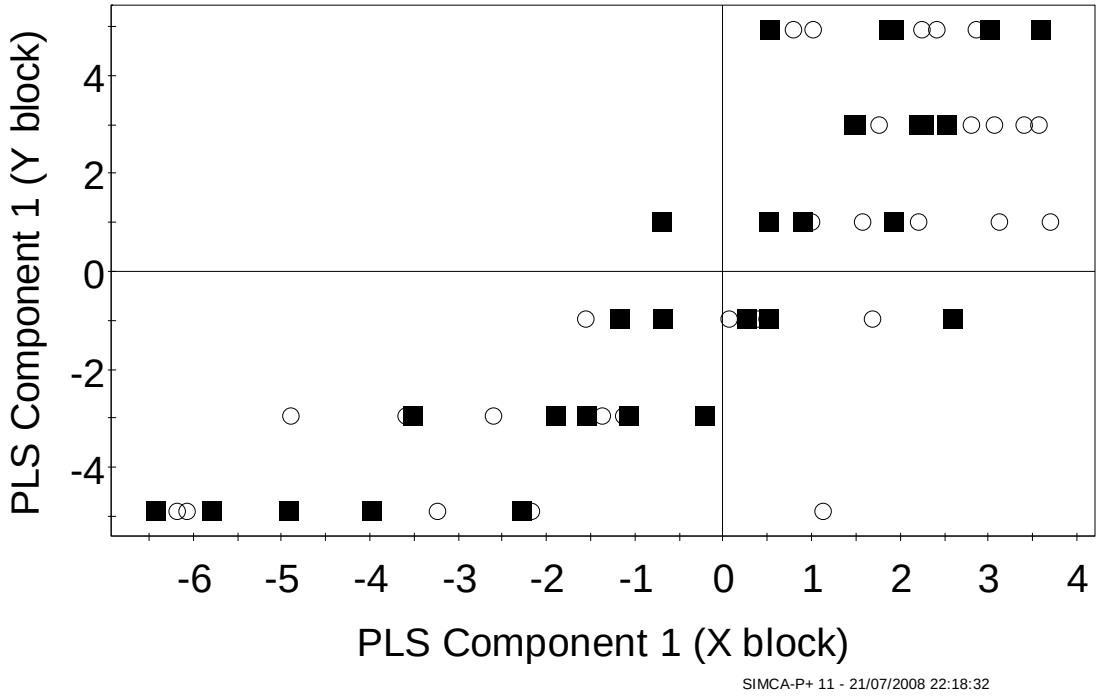

Fig 1b

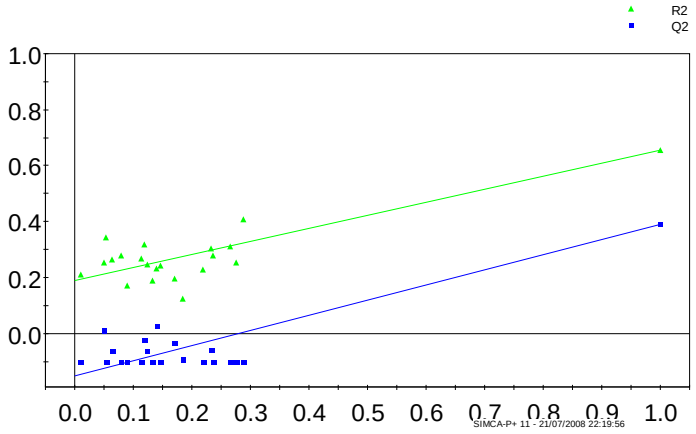

Fig 1c

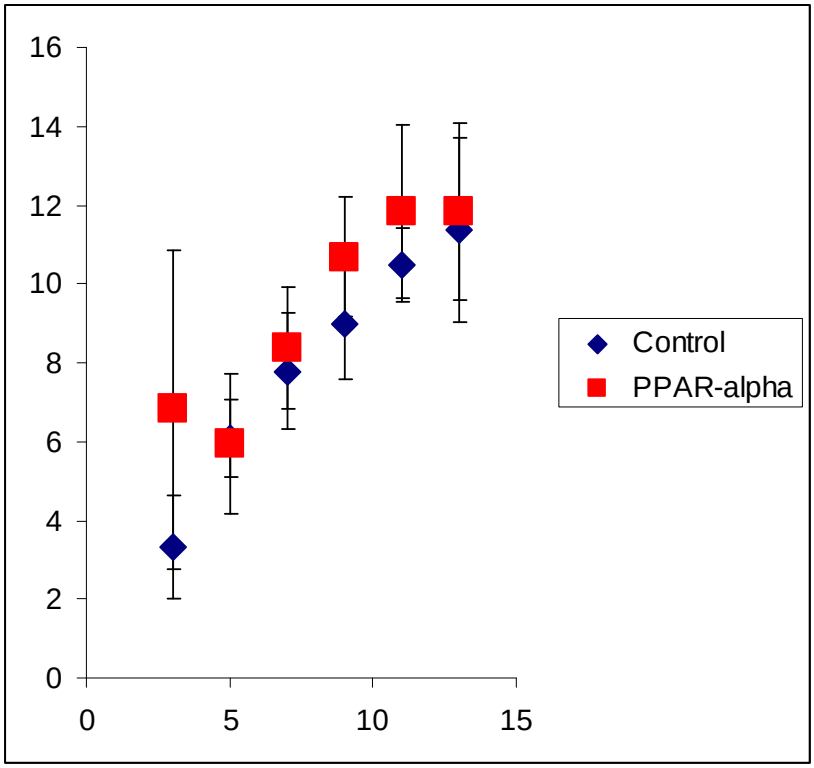

Supplementary Figure 1A: A PLS model formed by regression of age (Y axis) against the fatty acid profile of adipose tissue (X axis) from wildtype and PPAR-α null mice. **Key**: PPAR-α null (■); wild type (○) **B**: Cross validation of the PLS model in A formed by random permutations of the Y variable. **C**: A plot of actual age (X axis) against predicted age (Y) for a PLS model built using the wildtype fatty acid profiles to predict the age of the tissue of PPAR-α null mouse.

Age trend of fatty acid profiles in heart tissue

To examine how age influences the metabolic profile of the heart in wildtype and PPAR-α null mice PLS was applied to the whole, control and PPAR-α null fatty acid methyl ester datasets for this tissue. For all three datasets robust models were built (Q^2 = 0.71, 0.42 and 0.68, respectively) (**Sup Fig 2a & b** for combined dataset). Of the identified fatty acids, ageing was associated with decreases in the relative concentration of 20:0 eicosanoic acid, 11:0 undecanoic acid, 14:0 tetradecanoic acid and 15:0 pentadecanoic acid, and increases in 20:4 n-3 eicosatetraenoic acid, 20:3 n-3 eicosatrienoic acid and 20:2 n-6 eicosadienoic acid across the combined dataset.
The overall similarities between these groups were demonstrated by the fact that the PLS model formed by tissue from control mice was predictive for heart tissue from the PPAR-α null mouse (**Sup Fig 2c**).

Fig 2A:

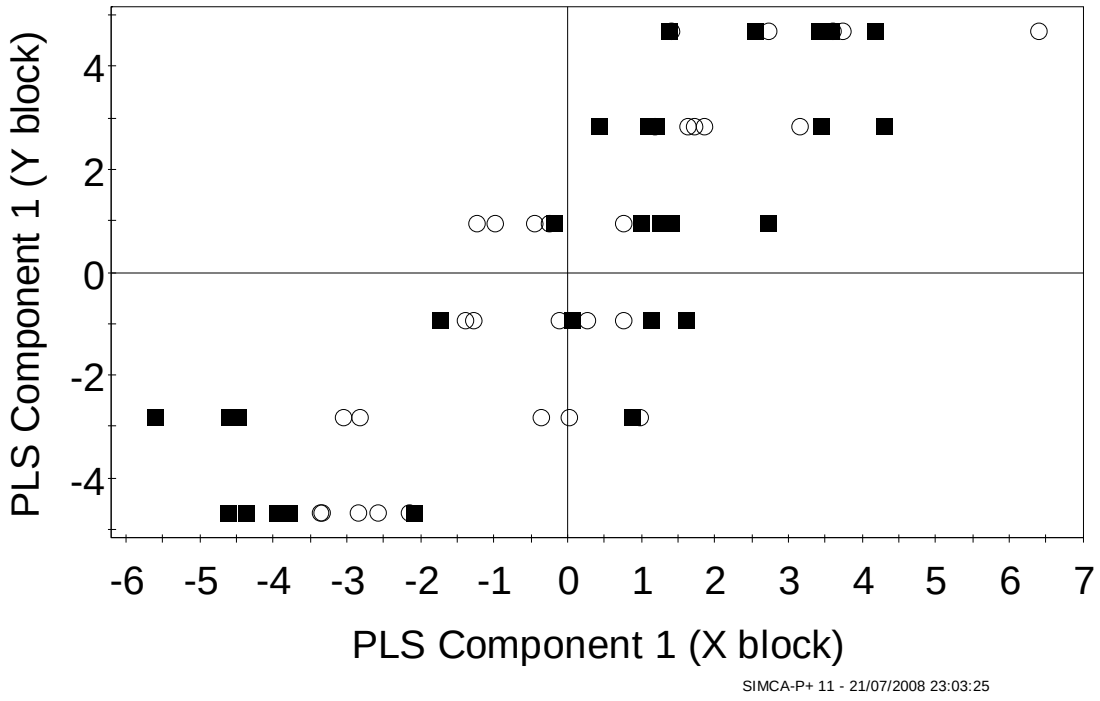

Fig 2B:

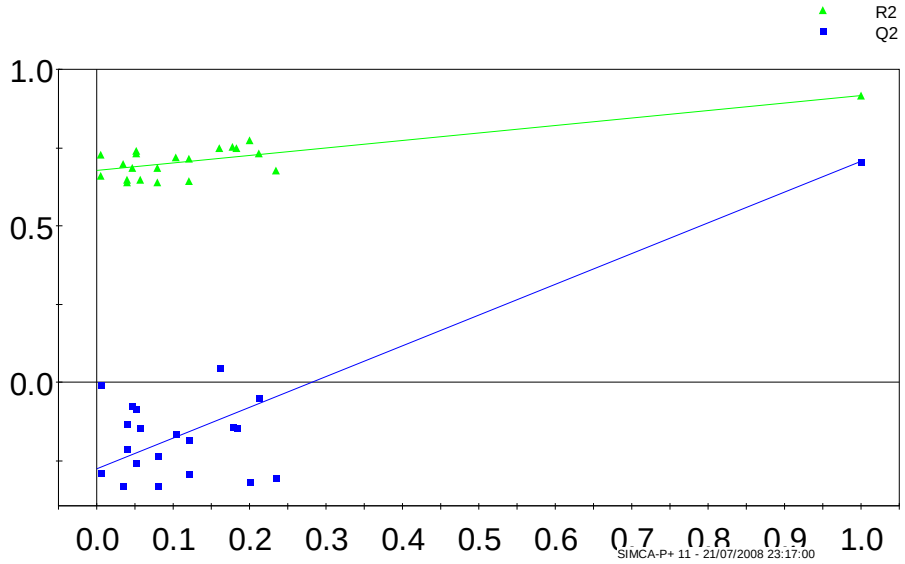

Fig 2c

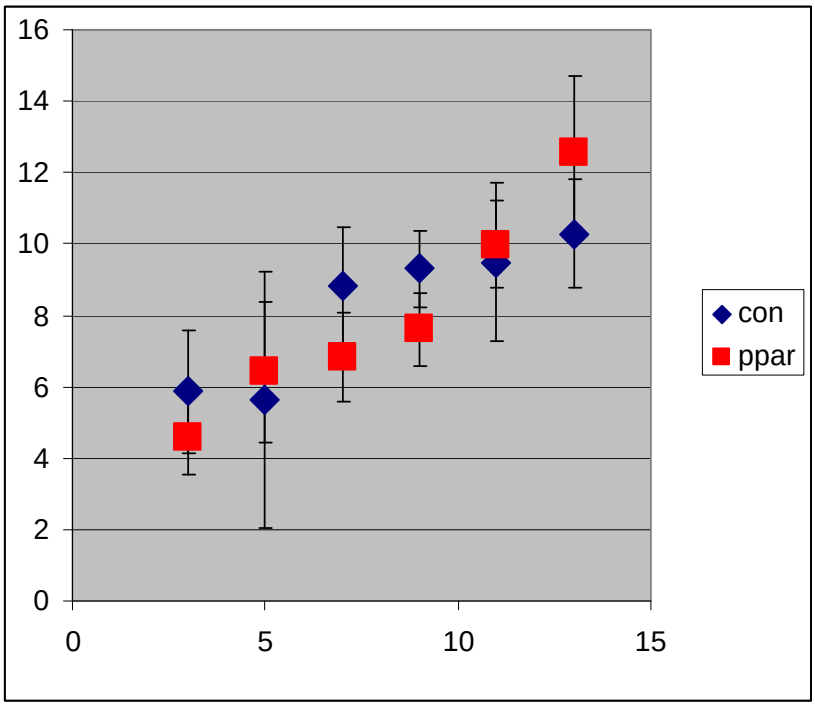

Supplementary Figure 2A: A PLS model formed by regression of age (Y axis) against the fatty acid profile of heart tissue (X axis) from wildtype and PPAR-α null mice. **Key**: PPAR-α null (■); wild type (○) **B**: Cross validation of the PLS model in A formed by random permutations of the Y variable. **C**: A plot of actual age (X axis) against predicted age (Y) for a PLS model built using the wildtype fatty acid profiles to predict the age of tissue from the PPAR-α null mouse.

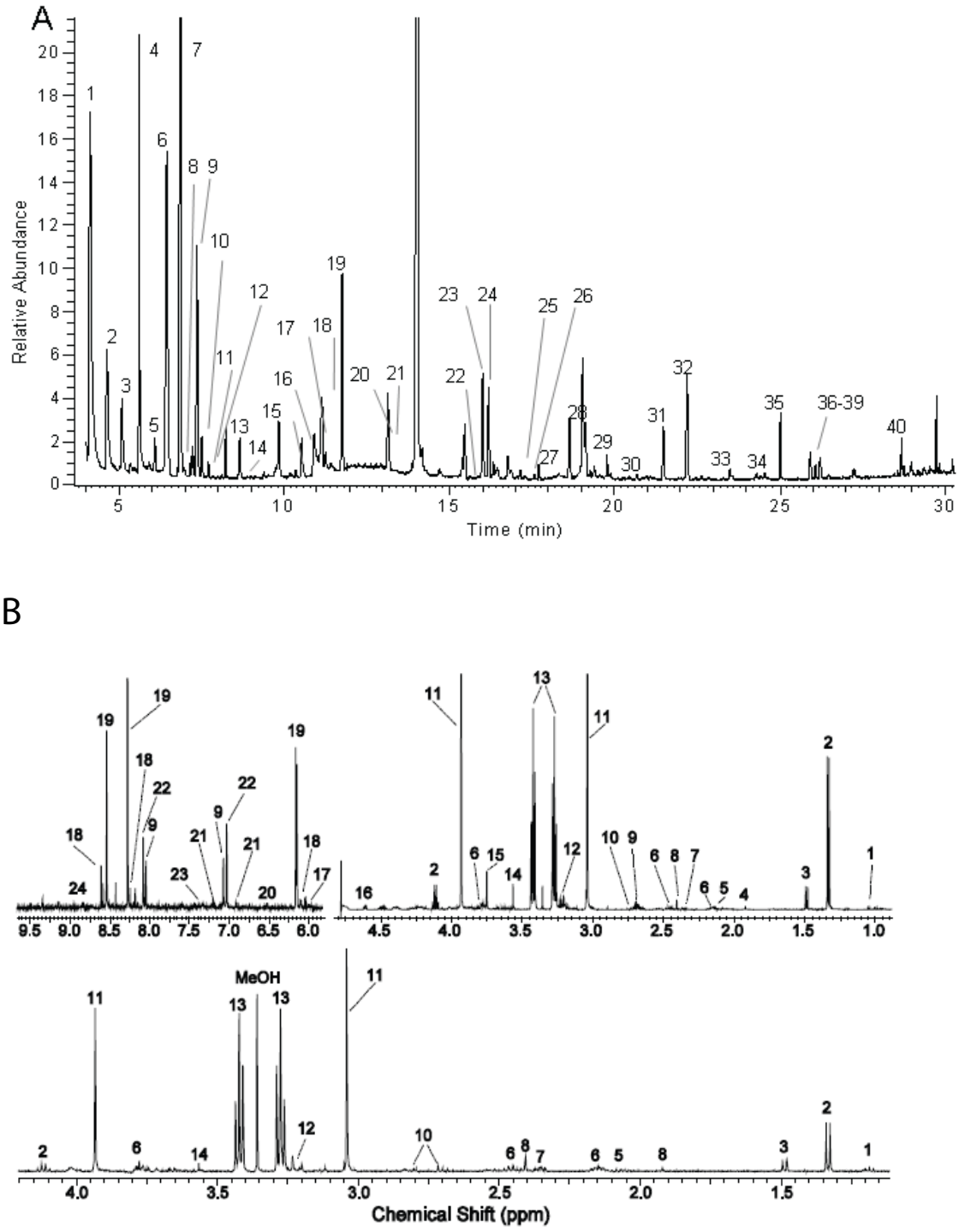

Supplementary Figure 3: (a) Annotated chromatogram showing some of the major aqueous soluble metabolites in 3 month control gastrocnemius tissue following TMS derivatisation and analysis by GC-MS. Key: (1) lactate, (2) alanine, (3) acetic acid, (4) urea , (5) valine, (6) urea, (7) phosphate, (8) leucine, (9) glycine, (10) proline, (11)

succinate, (12) fumarate, (13) serine, (14) threonine, (15) beta-alanine, (16) malate, (17) 5-oxo-proline, (18) hydroxyproline, (19) creatine, (20) glutamate, (21) phenylalanine, (22) ornithine, (23) phosphorylated sugar, (24) glutamine, (25) phosphoric acid, (26) citrate, (27) tyrosine, (28) glucose, (29) lysine, (30) ascorbate, (31) palmitic acid, (32) inositol isomer, (33) 9H-purine, (34) octadecenoic acid, (35) stearic acid, (36-39) disaccharides, (40) phosphorylated sugar. (b) Annotated 500 MHz ^{1}H NMR spectra of (A) gastrocnemius and (B) soleus skeletal muscle. The region δ 6.0-9.5 corresponds to an expansion of the aromatic region of spectrum A. Peak 1: valine/ leucine/ isoleucine, peak 2: lactate, peak 3: alanine, peak 4: acetate, peak 5: glutamate, peak 6: glutamate and glutamine, peak 7: malate, peak 8: succinate, peak 9: carnosine, peak 10: glutamine, peak 11: creatine, peak 12: cholines, peak 13: taurine, peak 14: glycine, peak 15: unassigned, peak 16: glucose, peak 17: GNP/ CNP/ UNP nucleotides, peak 18: adenosine, peak 19: ANPs, peak 20: fumarate, peak 21: tyrosine, peak 22: unassigned, peak 23: phenylalanine, peak 24: nicotinamide.

Gene expression changes in the 3 month PPAR-α null mouse

Sample preparation: The fibrous, original and lipid tissue RNeasy kits were used to extract total RNA from heart, liver and WAT samples, respectively (3 month; n=5 for each group) (Qiagen GmbH, Hilden, Germany). Gene expression was measured using 'RT^2 Profiler' arrays (Mouse Diabetes PCR Array; Superarray Bioscience Corporation, Frederick, MD; http://www.superarray.com/gene_array_product/HTML/OMM-023.html). Procedures were carried out according to manufacturer's instructions. Briefly, 1 μg of total RNA was reverse transcribed to cDNA then diluted and added to a master mix containing fluorescent SYBR Green dye. 25 μl aliquots of the mix were added to a 96-well plate containing pre-dispensed gene-specific primer sets in each well.
RT-PCR: The real time-PCR analysis was performed using an ABI Prism 7000 Sequence Detector System (Applied Biosystems, Foster City, CA). The amplification profile consisted of an initial incubation at 50^{o}C for 2 min, 95^{o}C for 10 min followed by 40 cycles of denaturation at 95^{o}C for 10 sec, annealing and extension at 60^{o}C for 1 min.
Data Analysis: The data were analysed quantitatively by measuring the threshold cycles (C_T) graphically using an amplification plot. C_T is the cycle at which a significant increase in fluorescence occurs; a C_T value below 40 indicates a positive result. The abundance of mRNA was normalised to the expression of β-actin. Data was exported into SIMCA-P 10.0 (Umetrics, Umeå, Sweden) for multivariate statistics.

Results: The expression of 84 genes, known to be associated with the onset or pathogenesis of diabetes mellitus, was measured in the heart, liver and adipose tissue of the PPAR-α null mouse using real time RT-PCR. Following application of PLS-DA to the data, PPAR-α null samples were readily distinguished from the control samples in all three tissues (**Supplementary figure 4**; Heart: $R^2(Y)=0.98$, $Q^2= 0.83$; Liver: $R^2(Y)=0.98$, $Q^2= 0.81$; Adipose: $R^2(Y)=0.89$, $Q^2= 0.53$). In the heart samples, the separation was attributed to an increase in *Nrf1*, *Ucp2*, *Pparg*, *Gpd1*, *Serpine1*, *Rab4a*, *Tgfb1*, and *Nos3*, and a decrease in *Adra1a* and *Pyg1*. In the liver there were significant increases in the expression of *Irs1* and *Icam1*, and decreased expression of *Pfkf3b*, *Ppargc1a*, *Pck1*, *G6pc*, *Ccr2*, and *Igfbp5*. In the adipose tissue there was an increase in the expression of

Mapk14, *Serpine1*, *Ccl5*, *Il6*, *Foxp3*, *Ptpn1*, *Irs1*, *Icam1*, *Gcgr*, *Gsk3b*, *Pik3r1*, *Tnfrs1b*, and *Tnfrs1a*.

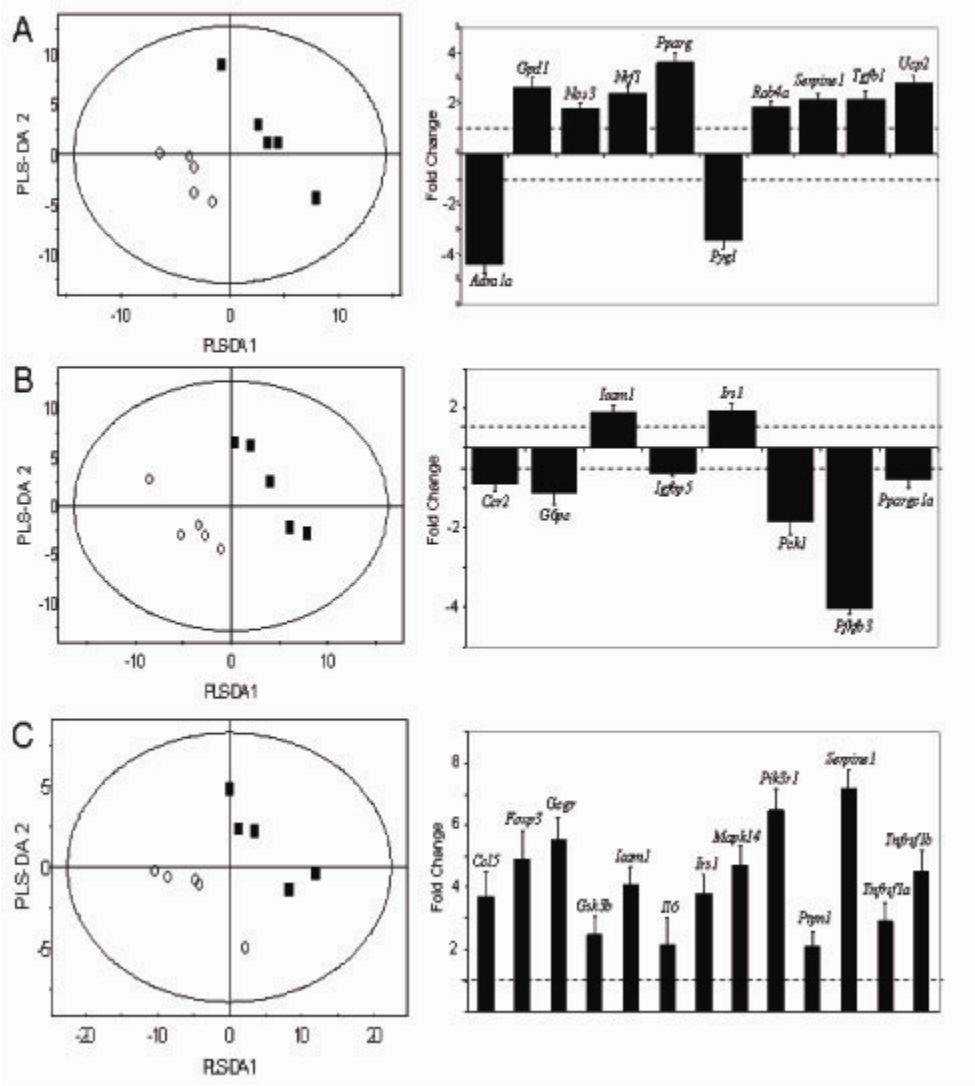

Supplementary Figure 4: PLS-DA score plots showing clustering of 3 month PPAR-α null (■) and control (○) samples following targeted transcriptomic analysis of (a) cardiac, (b) liver, and (c) white adipose tissue. Associated gene expression differences are shown in the adjoining plots which show the fold change of selected genes relative to expression levels in control samples.

Metabolic correlations between organs

Given the central role of the liver in regulating metabolism at the whole organism level and the large age and genotype associated differences in metabolism detected in the liver we investigated the correlation between metabolic changes in the liver and other tissues across the mouse genotypes and the time course. A PLS model was built with the X block

being formed by the integral regions of the NMR spectra of all tissues except the liver, while the Y-block was formed by the integral regions from the liver. Three datasets were considered: all animals, control strain only and PPAR-α null mice only. Robust PLS models were built for all three models (Q^2= 0.43 all data, 0.46 control, 0.50 PPAR-α null, respectively).

Examining the metabolites that were most correlated with the major metabolic changes in the liver by examining the loadings plot associated with each PLS model, an increase in glucose and glycogen in the liver was associated with increased concentrations of lactate, creatine, phosphocholine and taurine in gastroc tissue, and negatively correlated with aqueously soluble lipids in adipose tissue (largely free fatty acids) (Supplementary Figure 5). Similar loadings plots were formed for all three datasets.

Thus, in both genotypes there was a strong correlation between glucose and glycogen in the liver and lactate in skeletal muscle demonstrating the metabolic coupling between these organs as part of the Cori cycle. However, weaker correlates were found for heart and diaphragm. The concentrations of glucose and glycogen in the liver was also negatively correlated with aqueously soluble lipids in adipose tissue, demonstrating a coupling between hepatic and adipose metabolism that might in turn provide a mechanism by which the consequence of a failure to express PPAR-α in liver tissue affects adipose tissue, which does not normally express PPAR-α even in wildtype animals.

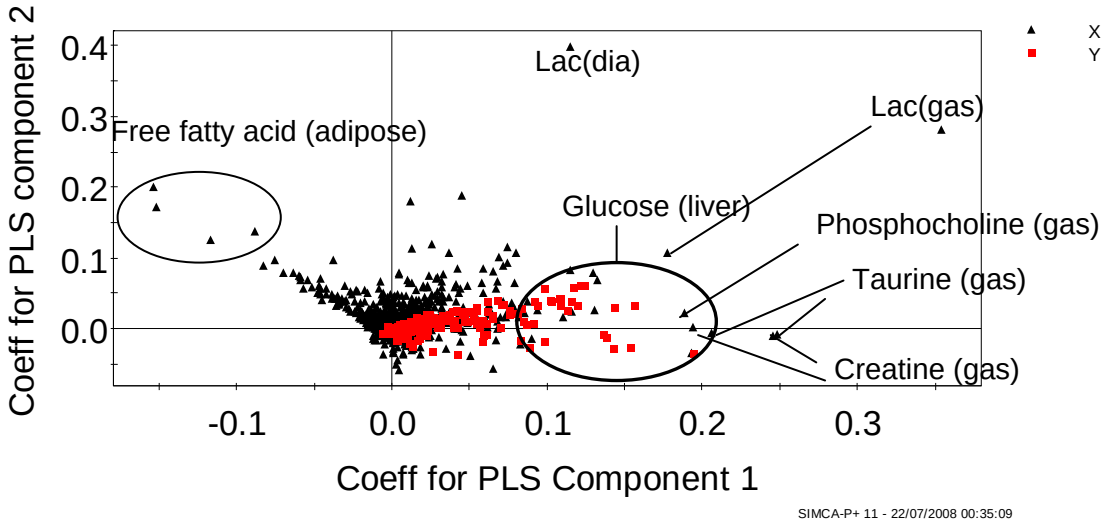

Supplementary Figure 5: The loadings plot for a PLS model formed between the NMR spectra from adipose, diaphragm, gastroc, soleus and heart tissue (X block) and the liver (Y block) to investigate metabolic correlations between tissues for both mouse genotypes. (Q^2= 0.43). Points in red represent spectral regions from spectra of liver tissue. Points in black represent spectral regions from spectra from the other tissues.

Determination of Coefficient of Variation for fatty acid analysis

A sample was analyzed by GC-FID for 7 times. The peaks are normalized to internal standard (D25-tridecanoic acid). The coefficient of variation (CV) for each FAME was calculated using the formula:

CV = standard deviation/mean for a normalized FAME peak

No.	FAME	CV
1	C10:0	0.030
2	C11:0	0.007
3	C12:0	0.003
5	C13:0	0.005
6	C14:0	0.009
7	C14:1_(cis-9)	0.011
8	C15:0	0.014
9	C16:0	0.013
10	C16:1_(cis-9)	0.017
11	C17:0	0.028
12	C18:0	0.028
13	C18:1_(trans-9)	0.016
14	C18:1_(cis-9)	0.026
15	C18:2_(trans-9,12)	0.035
16	C18:2_(cis-9,12)	0.029
17	C18:3_(cis-9,12,15)	0.034
18	C20:0	0.046
19	C20:1_(cis-11)	0.042
20	C22:0	0.053
21	C22:1_(cis-13)	0.044
22	C20:5_(cis-5,8,11,14,17)	0.037
23	C23:0	0.053
24	C24:0	0.054
25	C24:1_(cis-15)	0.056
26	C22:6_(cis-4,7,10,13,16,19)	0.050
	Average CV	0.02965

Determination of Coefficient of Variation for NMR spectroscopy analysis of aqueous extracts

Five aqueous extracts of mouse liver (50 mg wet weight) were produced using the chloroform/methanol extraction procedure described in Atherton et al., 2006. Extracts were dried and resuspended in phosphate buffered D_2O containing 1 mM TSP. Samples were analysed by a standard NOESYPR1D pulse sequence on a 500 MHz NMR spectrometer interfaced with a 11.74 T superconducting magnet. Spectra were acquired across 128 transients. Each time shimming was performed in automation using the au program topshim prior to data acquisition.

Spectra were integrated in automation using fixed width buckets of 0.02 ppm between 0.2 ppm and 9.8 ppm excluding the water containing region using ACD NMR manager. In addition the region 10-10.5 ppm was chosen as a region representing only noise. Data was normalised to total integral value across the regions integrated across. Within Excel all regions where the integral value was less than three times the noise level were excluded from further analysis. The coefficient of variation (CV) was calculated for assigned metabolites using the formula:

CV = standard deviation/mean for a given bucket region.

(ppm)	CV	
[1.00 .. 1.02]	0.19	leucine, isoleucine, valine
[1.20 .. 1.22]	0.10	beta-hydroxybutyrate
[1.32 .. 1.34]	0.10	lactate
[1.46 .. 1.48]	0.012	alanine
[1.90 .. 1.92]	0.18	acetate
[2.34 .. 2.36]	0.14	glu
[2.44 .. 2.46]	0.12	gln
[3.00 .. 3.02]	0.13	lysine
[3.04 .. 3.06]	0.063	creatine
[3.20 .. 3.22]	0.060	choline
[3.24-3.26]	0.047	TMAO/betaine
[3.86-3.88]	0.026	betaine
[3.22 .. 3.24]	0.045	phosphocholine
[3.54 .. 3.56]	0.014	gluc
[3.90 .. 3.92]	0.026	creatine
[5.38 .. 5.40]	0.091	glycogen
[8.32 .. 8.34]	0.16	adenosine
Average	0.088	